



The role of fluorine in granite-related hydrothermal tungsten ore genesis: Results of experiments and modeling

Xin-Song Wang^{a,b,*}, A.E. Williams-Jones^b, Rui-Zhong Hu^a,
Lin-Bo Shang^a, Xian-Wu Bi^a

^a State Key Laboratory of Ore Deposits Geochemistry, Institute of Geochemistry, Chinese Academy of Sciences, Guiyang 550002, China

^b Department of Earth and Planetary Sciences, McGill University, 3450 University Street, Montreal, QC H3A 0E8, Canada

Received 19 May 2020; accepted in revised form 25 September 2020; Available online 6 October 2020

Abstract

Most of the World's large tungsten deposits are genetically related to fluorine-rich granitic magmas, their ores contain fluorine minerals, such as fluorite and topaz, and their host rocks have commonly undergone fluorine metasomatism to form greisens. In view of this evidence that tungsten ore fluids are enriched in fluorine, and the potential for fluoride to form stable complexes with hard acids (e.g., W^{6+}), we investigated the solubility and speciation of tungsten in fluoride-bearing fluids at hydrothermal conditions. Experiments were conducted to measure the solubility of tungsten trioxide solid in fluoride-bearing aqueous fluids at temperatures between 100 and 250 °C and vapour-saturated water pressure. Based on the results of these experiments, tungsten is dissolved predominantly as $H_3WO_4F_2^-$ in solutions containing 0.05–0.30 m HF at pH(T) values between 1.5 and 3.4. Significantly, the concentration of $H_3WO_4F_2^-$ was up to two orders of magnitude higher than that of tungstate species in these experimental solutions. This species formed via the reaction $WO_3^{cryst} + H_2O + 2HF = H_3WO_4F_2^- + H^+$, logarithms of the equilibrium constants for which, vary from -4.39 ± 0.18 at 100 °C to -5.10 ± 0.17 at 250 °C. In solutions containing <0.05 m HF, the dominant species is $H_2WO_4^0$. Fluid-rock interaction models employing these data predict that fluorine-bearing fluids will deposit ten times the mass of tungsten at a given fluid-rock ratio than fluorine-free hydrothermal fluids (the latter models consistently underestimate tungsten deposit grades). They also successfully explain why wolframite and not scheelite is the major tungsten mineral in vein- and greisen-type granite-hosted deposits, showing that calcium released to the fluid is consumed to form fluorite, thereby precluding saturation of the fluid with scheelite. The occurrence of fluorite in tungsten deposits is therefore not coincidental but instead a byproduct of the mineralizing process.

© 2020 Elsevier Ltd. All rights reserved.

Keywords: Hydrothermal experiments; Tungsten solubility and speciation; Fluoride; Tungsten ore formation

1. INTRODUCTION

Tungsten is a relatively rare critical metal that has become an essential component of many of the superalloys being developed for advanced technologies (Hayes and McCullough, 2018). It is also a metal of major strategic importance because ~50% of the global supply of tungsten

is from deposits in South China (Hu and Zhou, 2012). Thus, there is considerable impetus to better understand the geochemical controls on the mobility of this metal and its concentration in the Earth's crust. An important feature of all large tungsten deposits is that they are genetically related to highly fractionated F-rich granites. Another is that the tungsten mineralization is commonly associated with greisenization, an alteration-type characterized by topaz, and/or fluorine-rich mica and fluorite (Polya, 1989; Heinrich, 1990; Lu et al., 2003; Romer and Lüders,

* Corresponding author.

E-mail address: wangxinsong@mail.gyig.ac.cn (X.-S. Wang).

2006; Wei et al., 2012; Lecumberri-Sanchez et al., 2017; Wu et al., 2017; Song et al., 2018; Pan et al., 2019). These features suggest that fluorine may play an important role in the transport of tungsten, a suggestion which is supported by the observation that fluoride is a hard ligand and should therefore have the potential to form strong complexes with a hard metal ion like W^{6+} (Williams-Jones and Migdisov, 2014).

Despite the above observations, it is widely accepted that tungsten is transported in hydrothermal fluids mainly as tungstic acid ($H_2WO_4^0$) and its dissociation products (HWO_4^- , and WO_4^{2-}), the stability of which has been determined reliably through experiments (Wesolowski et al., 1984; Wood and Vlassopoulos, 1989; Wood, 1992; Wang et al., 2019, 2020). Some studies have proposed that pairing of the tungstate ion with Na^+ (Wood and Vlassopoulos, 1989; Wood and Samson, 2000) or chloride complexation (Manning and Henderson, 1984) may also be important in tungsten speciation at elevated temperature. The results of our recent study of the solubility of tungsten trioxide solid in NaCl-bearing solutions, however, do not support either proposal (Wang et al., 2019).

Although several studies have proposed that tungsten may be transported hydrothermally by fluoride and oxyfluoride complexes, such as WF_6 , $W_2O_2F_8$, $WO_3F_2^{2-}$ and $WO_2F_4^{2-}$ (Schröcke et al., 1984; Liu and Ma, 1987; Song

et al., 2018), to our knowledge, the hypothesis that tungsten could be transported as a fluoride-bearing species has not been investigated experimentally. Moreover, the only potentially relevant experimental study, which investigated the partitioning of tungsten between a haplogranitic magma and a HF-bearing fluid, concluded that HF has no effect on this partitioning (Keppler and Wyllie, 1991). For these reasons, and those presented earlier, there is, thus, a pressing need for experimental data that rigorously determine whether or not fluoride ions form stable complexes with aqueous tungsten species at hydrothermal conditions.

Here, we report results of experiments designed to evaluate tungsten solubility and speciation in the system NaF-HCl-NaCl-H₂O at temperatures between 100 and 250 °C, vapor-saturated water pressure and acidic pH. The results show that $H_3WO_4F_2^-$ is the dominant species at high HF concentration, and tungstic acid ($H_2WO_4^0$) is the dominant tungsten species at low pH and low HF concentration. We retrieve thermodynamic data for $H_3WO_4F_2^-$ and $H_2WO_4^0$ from these results and use them to evaluate the solubility of scheelite and wolframite in HF-rich hydrothermal fluids. The results indicate that fluorine plays an essential role in the formation of tungsten deposits, they explain why wolframite is the dominant ore mineral in vein and greisen granite-hosted tungsten deposits and they show that fluorite in these deposits is genetically related to the tungsten mineralization.

2. METHODS

2.1. Experiments

The experimental equipment and methods adopted in this study are the same as those used in previous studies at McGill University (Migdisov and Williams-Jones, 2007; Timofeev et al., 2017; Wang et al., 2019). The experiments were carried out in Teflon test tubes, which were placed in batch-type titanium grade 2 autoclaves (Fig. 1) and heated in a Fisher Isotemp oven equipped with a stainless-steel box to reduce thermal gradients. Prior to each experiment, the Teflon test tubes were cleaned by filling them with a 3 wt. % ammonium hydroxide (trace metal grade) solution, allowing them to stand for 12 hours, and then washing them with nano-pure water. This treatment ensured that any tungsten remaining on the walls of the tubes from previous experiments was removed.

The solubility of tungsten (VI) trioxide solid was investigated in 0.5 m NaCl aqueous solutions of variable HF concentration and pH at temperatures of 100, 125, 150, 175, 200, 225, and 250 °C, and vapor-saturated water pressure. The HF solutions were prepared by adding NaF solid to nano-pure water in amounts that yielded fluoride concentrations ranging from 0.005 mol/kg to 0.3 mol/kg; the pH of the solutions was controlled by adding HCl and varied from 1.16 to 2.36 at ambient temperature. Solid reactant (WO_3 , yellow powder; Alfa Aesar 99.998% purity) was introduced into a small Teflon holder (~3 cm long) that was then capped by Teflon wool to prevent mechanical transfer of the solid to the solution. In order to ensure that

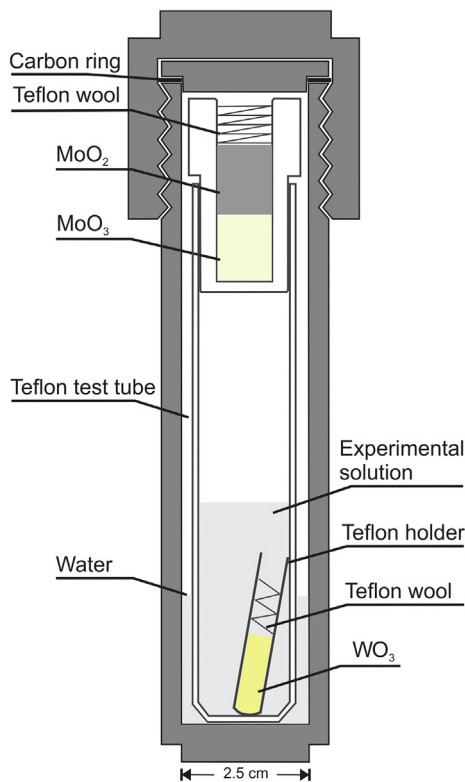


Fig. 1. An illustration showing the experimental set-up employed in this study. A hole was drilled into the top of the Teflon cap of the reactor, which was filled by MoO_3 and MoO_2 powder to control the oxygen fugacity of the fluid. Malleable carbon rings provided an airtight seal upon closure of the autoclave.

the experiments were conducted at conditions for which the tungsten would be in the 6+ state, the oxygen fugacity of the solutions was buffered by MoO₃ (light yellow powder; Alfa Aesar 99.95% purity) and MoO₂ (brown powder; Alfa Aesar, 99% purity), which were introduced into the top of the Teflon reactor (Fig. 1). At the beginning of each experiment, the teflon reactor was placed in an autoclave and 12 ml of HF-bearing NaCl solution was added to it (Fig. 1). Prior to sealing, the reactor was purged with nitrogen gas to remove atmospheric oxygen, and 0.8 ml of nanopure water was added to the autoclave (Fig. 1) to balance the pressure developed inside the reactor during the experiments with the pressure in the autoclaves.

Kinetic experiments were performed at 100 °C with a 0.5 mol/kg NaCl solution containing 0.27 mol/kg HF and 0.26 mol/kg HCl for durations between 1 and 11 days. The tungsten concentration reached a steady state value after 6 days (Fig. 2). As experiments conducted at higher temperature were predicted to reach steady state concentrations more rapidly, all subsequent experiments were conducted for durations of ≥ 7 days. At the end of each set of experiments, the autoclaves were removed from the oven and quenched in water to ambient temperature in less than 20 minutes. A 2 ml aliquot of solution was taken from each tube for pH determination and analysis of the fluoride concentration. One ml of concentrated trace metal grade hydrofluoric acid was then added to each tube to dissolve any tungsten that had precipitated on the walls of the reactor during quenching. After 30 minutes, the mixed solution was removed for analysis of its tungsten content. The pH and fluoride concentration were measured using an InLab™ Hydrofluoric Electrode and Thermo Scientific™ Orion™ Fluoride Electrode purchased from Fisher Scientific. Solutions containing greater than 0.1 mol/kg Na⁺ and 0.01 mol/kg HF were diluted with distilled water prior to measuring their pH. The resulting pH values were corrected to pH values corresponding to the temperatures of the

experiments using HCh software (Shvarov, 2008). Tungsten concentrations were analyzed using Inductively Coupled Plasma Mass Spectrometry after 2500 to 40,000 times dilution of the experimental solution using a mixture of 2 wt.% HCl and 0.001 wt.% HF solution. Finally, the WO₃ reactant was analyzed by X-ray diffraction to confirm that no new solids had formed during the experiments and that the measured solubility corresponded only to the dissolution of WO₃^{cryst}; the sole phase detected was crystalline WO₃. X-ray diffraction analysis also confirmed that the buffer solids, MoO₂ and Mo₂O₃, were both present after the experiments. Moreover, the colorless nature of the quenched solution shows that the buffer operated as desired and that W was exclusively in the 6+ oxidation state; even traces of W in lower oxidation states would have imparted a blue color to the solution.

2.2. Data optimization

The tungsten species in the solution were identified from the slope of the logarithm of the molality of tungsten with respect to that of other ions in each experiment. The standard Gibbs free energy of formation of these species, ΔG°_f , was determined from the molality of tungsten, NaF, NaCl and HCl in each experiment using the program OptimA (masses corresponding to an excess of the solute, WO₃^{cryst}, and of each phase in the oxygen buffer assemblage, at the end of each experiment, were also specified in the input file), which is part of the HCh software package (Shvarov, 2015). The activity coefficient of each ionic species at the different experimental conditions was calculated using the extended Debye-Hückel equation (Helgeson et al., 1981; Oelkers and Helgeson, 1990, 1991):

$$\log \gamma_n = -\frac{A \cdot [z_n]^2 \cdot \sqrt{I}}{1 + B \cdot a \cdot \sqrt{I}} + b_\gamma \cdot I + \Gamma \quad (1)$$

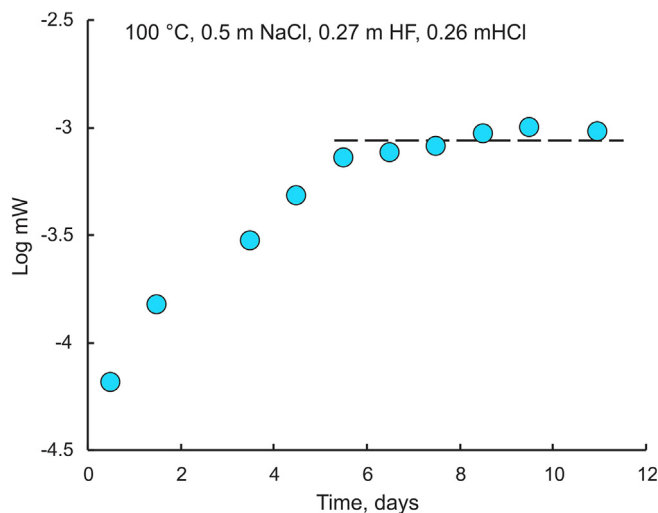


Fig. 2. A plot of tungsten concentration versus time showing the results of experiments of variable duration conducted at 100 °C (kinetic experiments) with an aqueous solution containing 0.5 mol/kg NaCl, 0.27 mol/kg HF and 0.26 mol/kg HCl. From this plot, it is evident that the solubility of WO₃^{cryst} reached a steady state concentration after 6 days.

Table 1
Compositions of the quenched experimental solutions. The values of pH (T) were calculated for the temperatures of interest.

T (°C)	NaCl(m)	HCl(m), 10 ⁻³	HF(m), 10 ⁻³	W(m), 10 ⁻⁶	pH (25 °C)	pH (T)
250	0.50	89.4	44.9	7.46	1.53	1.80
250	0.50	126	18.1	13.7	1.16	1.42
250	0.50	107	32.4	11.4	1.32	1.58
250	0.50	49.2	25.6	11.9	1.80	2.06
250	0.50	22.4	18.4	19.8	2.31	2.81
250	0.50	28.8	19.1	24.9	2.12	2.44
250	0.50	26.7	19.9	12.7	2.21	2.59
250	0.50	33.0	27.4	14.1	2.20	2.67
250	0.50	34.4	31.0	28.4	2.27	2.87
250	0.50	43.9	39.8	34.5	2.21	2.79
250	0.50	54.4	48.4	26.0	2.11	2.65
250	0.50	56.8	47.5	25.6	2.04	2.46
250	0.50	67.2	58.4	31.4	2.03	2.49
250	0.50	121	104	60.1	1.82	2.20
250	0.50	192	176	228	1.78	2.25
250	0.50	101	95.3	47.4	2.01	2.63
250	0.50	152	141	177	1.89	2.43
250	0.50	172	164	113	1.90	2.54
250	0.50	236	231	455	1.88	2.68
250	0.50	228	229	766	1.94	3.04
250	0.50	274	249	118	1.65	2.07
250	1.00	254	244	259	1.81	2.47
250	0.50	210	155	26.9	1.43	1.73
250	0.50	186	154	34.5	1.63	1.97
250	0.50	181	160	58.5	1.74	2.15
250	0.50	172	164	113	1.90	2.54
225	0.50	114	8.22	4.42	1.17	1.35
225	0.50	49.3	8.99	6.47	1.58	1.76
225	0.50	35.0	10.56	6.50	1.79	1.97
225	0.50	18.0	13.2	16.0	2.34	2.67
225	0.50	11.6	3.84	6.83	2.27	2.47
225	0.50	29.8	18.3	18.3	2.06	2.30
225	0.50	43.2	36.5	19.3	2.14	2.52
225	0.50	60.0	50.9	16.0	2.04	2.40
225	0.50	72.3	63.2	32.5	2.02	2.40
225	0.50	79.8	78.1	162	2.14	2.91
225	0.50	87.3	80.6	36.3	2.03	2.51
225	0.50	128	116	50.9	1.88	2.28
225	0.50	209	199	257	1.84	2.36
225	0.50	164	159	168	1.94	2.56
225	0.50	249	224	140	1.66	1.99
225	0.50	310	297	928	1.74	2.24
225	0.50	238	236	792	1.90	2.71
225	0.50	224	229	1143	2.00	3.15
225	0.50	164	159	168	1.94	2.56
225	0.50	223	167	43.1	1.42	1.64
225	0.50	194	160	46.8	1.61	1.87
225	0.50	177	159	96.6	1.76	2.11
225	0.50	163	155	204	1.90	2.43
225	0.50	141	141	429	2.05	2.97
200	0.50	113	8.71	5.64	1.18	1.31
200	0.50	80.3	11.4	3.07	1.35	1.48
200	0.50	52.3	11.7	2.61	1.58	1.71
200	0.50	35.0	10.0	2.73	1.78	1.91
200	0.50	11.9	3.93	3.59	2.25	2.40
200	0.50	13.9	6.07	3.99	2.25	2.41
200	0.50	26.8	17.2	5.35	2.12	2.33
200	0.50	15.8	11.2	7.86	2.36	2.64
200	0.50	33.7	23.2	5.77	2.08	2.29
200	0.50	41.7	27.1	7.49	1.97	2.15

(continued on next page)

Table 1 (continued)

T (°C)	NaCl(m)	HCl(m), 10 ⁻³	HF(m), 10 ⁻³	W(m), 10 ⁻⁶	pH (25 °C)	pH (T)
200	0.50	33.1	32.0	24.3	2.35	3.00
200	0.50	41.1	38.8	16.8	2.27	2.84
200	0.50	34.8	32.2	13.8	2.29	2.81
200	0.50	61.3	52.1	23.0	2.04	2.34
200	0.50	49.6	42.4	18.2	2.11	2.44
200	0.50	74.1	64.7	30.5	2.01	2.32
200	0.50	82.1	81.4	138	2.16	2.90
200	0.50	134	118	60.2	1.83	2.11
200	0.50	86.5	81.5	38.4	2.06	2.55
200	0.50	159	149	305	1.88	2.27
200	0.50	203	192	365	1.84	2.26
200	0.50	305	291	1110	1.74	2.17
200	0.50	170	157	153	1.85	2.21
200	0.50	235	215	202	1.72	2.02
200	0.50	218	215	522	1.91	2.57
200	0.50	215	217	902	1.98	2.87
200	0.50	213	225	1393	2.08	3.22
200	0.50	170	157	153	1.85	2.21
200	0.50	212	150	40.7	1.39	1.54
200	0.50	195	157	51.7	1.56	1.74
200	0.50	177	154	81.4	1.71	1.96
200	0.50	164	166	307	2.04	2.93
175	0.50	117	8.55	3.73	1.16	1.25
175	0.50	52.3	9.59	4.60	1.56	1.65
175	0.50	37.2	10.2	6.29	1.75	1.84
175	0.50	18.5	14.0	8.66	2.34	2.59
175	0.50	9.27	1.41	1.77	2.28	2.38
175	0.50	29.9	20.8	14.7	2.13	2.31
175	0.50	48.3	42.8	24.2	2.16	2.49
175	0.50	61.8	54.9	30.1	2.08	2.40
175	0.50	129	117	69.6	1.89	2.18
175	0.50	73.5	67.2	39.9	2.07	2.42
175	0.50	80.0	83.1	165	2.23	3.07
175	0.50	88.0	81.8	52.7	2.04	2.42
175	0.50	203	194	336	1.86	2.28
175	0.50	166	160	247	1.93	2.37
175	0.50	228	222	619	1.87	2.36
175	0.50	246	223	237	1.68	1.91
175	0.50	226	228	915	1.97	2.69
175	0.50	220	232	1257	2.08	3.04
175	0.50	211	238	2062	2.24	3.35
175	0.50	233	168	63.0	1.37	1.48
175	0.50	211	171	87.5	1.54	1.69
175	0.50	194	171	130	1.71	1.92
175	0.50	184	172	233	1.84	2.17
175	0.50	176	166	201	1.87	2.24
175	0.50	173	174	335	2.02	2.73
150	0.50	116	8.00	0.97	1.16	1.22
150	0.50	77.3	8.45	1.29	1.36	1.41
150	0.50	52.0	9.03	0.70	1.56	1.62
150	0.50	34.2	8.48	1.47	1.77	1.84
150	0.50	9.36	1.18	0.47	2.27	2.33
150	0.50	12.8	4.58	0.96	2.24	2.33
150	0.50	16.5	11.16	2.87	2.33	2.50
150	0.50	29.6	19.71	4.99	2.11	2.24
150	0.50	53.4	44.6	21.1	2.06	2.27
150	0.50	63.8	54.2	37.7	2.02	2.23
150	0.50	72.4	62.7	39.7	2.00	2.23
150	0.50	143	128	123	1.84	2.06
150	0.50	87.5	87.9	115	2.16	2.72
150	0.50	86.6	79.3	50.8	2.02	2.31

(continued on next page)

Table 1 (continued)

T (°C)	NaCl(m)	HCl(m), 10 ⁻³	HF(m), 10 ⁻³	W(m), 10 ⁻⁶	pH (25 °C)	pH (T)
150	0.50	184	175	326	1.87	2.18
150	0.50	228	214	466	1.79	2.06
150	0.50	185	173	203	1.83	2.11
150	0.50	259	253	836	1.85	2.27
150	0.50	279	250	249	1.62	1.79
150	0.50	250	256	918	1.98	2.64
150	0.50	238	174	57.0	1.37	1.46
150	0.50	213	174	80.2	1.56	1.67
150	0.50	197	174	104	1.70	1.87
150	0.50	185	173	203	1.83	2.11
150	0.50	173	176	401	2.03	2.64
125	0.50	118	9.57	1.92	1.16	1.20
125	0.50	52.1	10.9	9.23	1.57	1.61
125	0.50	35.3	10.2	2.76	1.78	1.82
125	0.50	18.2	13.4	5.37	2.34	2.50
125	0.50	10.0	1.77	3.18	2.26	2.30
125	0.50	34.3	23.5	3.26	2.07	2.17
125	0.50	30.1	26.2	7.93	2.28	2.52
125	0.50	35.7	25.7	4.86	2.08	2.20
125	0.50	43.7	26.9	4.34	1.92	1.99
125	0.50	36.1	31.8	12.3	2.24	2.48
125	0.50	46.7	43.8	13.1	2.23	2.54
125	0.50	56.8	48.5	13.0	2.07	2.25
125	0.50	70.0	60.1	24.9	2.01	2.18
125	0.50	84.8	73.7	30.0	1.96	2.13
125	0.50	102.4	92.1	57.7	1.94	2.15
125	0.50	148	133	101	1.83	2.00
125	0.50	188	182	281	1.90	2.20
125	0.50	235	223	335	1.80	2.04
125	0.50	289	259	349	1.61	1.74
125	0.50	272	257	813	1.75	1.98
125	0.50	186	177	277	1.87	2.14
125	0.50	238	174	63.8	1.37	1.43
125	0.50	214	176	108	1.55	1.64
125	0.50	196	174	188	1.72	1.87
125	0.50	188	182	281	1.90	2.20
125	0.50	178	181	347	2.03	2.52
100	0.50	118	9.05	0.43	1.16	1.18
100	0.50	53.5	10.2	0.48	1.55	1.57
100	0.50	36.1	9.86	1.60	1.76	1.79
100	0.50	18.0	12.9	0.81	2.33	2.44
100	0.50	9.35	1.28	0.27	2.27	2.30
100	0.50	31.6	21.9	4.42	2.10	2.19
100	0.50	30.6	26.2	13.1	2.26	2.44
100	0.50	37.1	25.0	2.74	2.03	2.10
100	0.50	45.8	26.7	4.05	1.87	1.92
100	0.50	54.0	47.0	12.5	2.10	2.26
100	0.50	67.7	59.0	17.7	2.03	2.18
100	0.50	80.8	72.1	27.8	2.01	2.16
100	0.50	99.3	91.5	64.7	1.99	2.18
100	0.50	149	135	99.5	1.84	1.99
100	0.50	188	178	311	1.87	2.07
100	0.50	232	219	429	1.79	1.97
100	0.50	89.2	89.8	48.3	2.16	2.48
100	0.50	192	179	244	1.82	1.99
100	0.50	269	254	575	1.75	1.92
100	0.50	287	254	429	1.58	1.67
100	0.50	253	260	1036	1.99	2.37
100	0.50	192	179	244	1.82	1.99
100	0.50	237	177	72.5	1.40	1.43
100	0.50	217	178	96.5	1.55	1.61
100	0.50	203	179	171	1.69	1.79
100	0.50	180	182	354	2.02	2.35

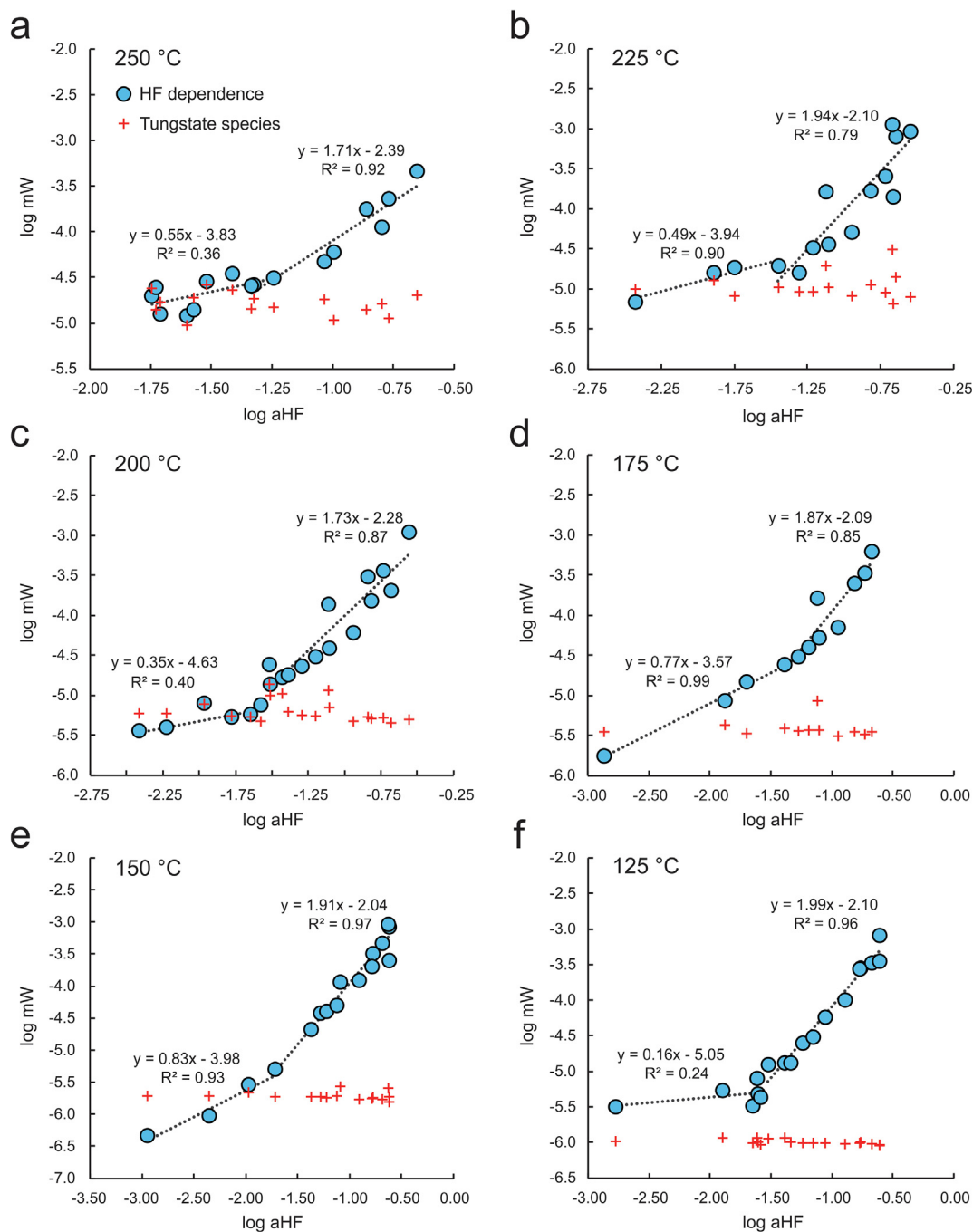


Fig. 3. Results of experiments at 250–125 °C showing the concentrations of dissolved tungsten (log mW) as a function of the activity of HF (log aHF). The filled blue circles record the results of experiments designed to determine the dependence of the solubility of $\text{WO}_3^{\text{cyst}}$ on HF molality at a $\text{pH}_{(25\text{ }^\circ\text{C})}$ of ~ 2 . The red crosses represent the concentration of tungstate species (H_2WO_4^0 , HWO_4^- and WO_4^{2-}), which were calculated for the experimental conditions using thermodynamic data from Wang et al. (2019) and Shock et al. (1997). The equations “ $y = ax - b$ ” represent linear regressions of the data. The results of experiments conducted at 100 °C are illustrated in Fig. 3g of Appendix 1.

in which A and B are constants representing Debye-Hückel limiting law parameters, b_γ is the extended parameter for NaCl from Helgeson and Kirkham (1974), a is the distance of closest approach, which is specific to the ion of interest, z is the charge of the ion, Γ is a molarity to molality

conversion factor, and I is the ionic strength calculated using Eq. (2):

$$I = \frac{1}{2} \sum_{i=1}^n c_i z_i^2 \quad (2)$$

where c_i is the molar concentration of ion i (mol/kg) and z_i is the charge of that ion. Parameter I represents the true ionic strength as all the dissolved components were considered. The activity coefficients of neutral species were assumed to be unity. The Haar-Gallagher-Kell and Marshall and Franck models were used to determine the thermodynamic properties and disassociation constant of H_2O , respectively, for our experimental conditions (Marshall and Franck, 1981; Kestin et al., 1984).

3. RESULTS

3.1. Identification of the dissolved tungsten species

The results of the experiments are reported in Table 1. In order to determine whether or not tungsten solubility depends on HF concentration, sets of experiments were conducted with solutions having roughly constant pH (~ 2) at ambient temperature and variable HF

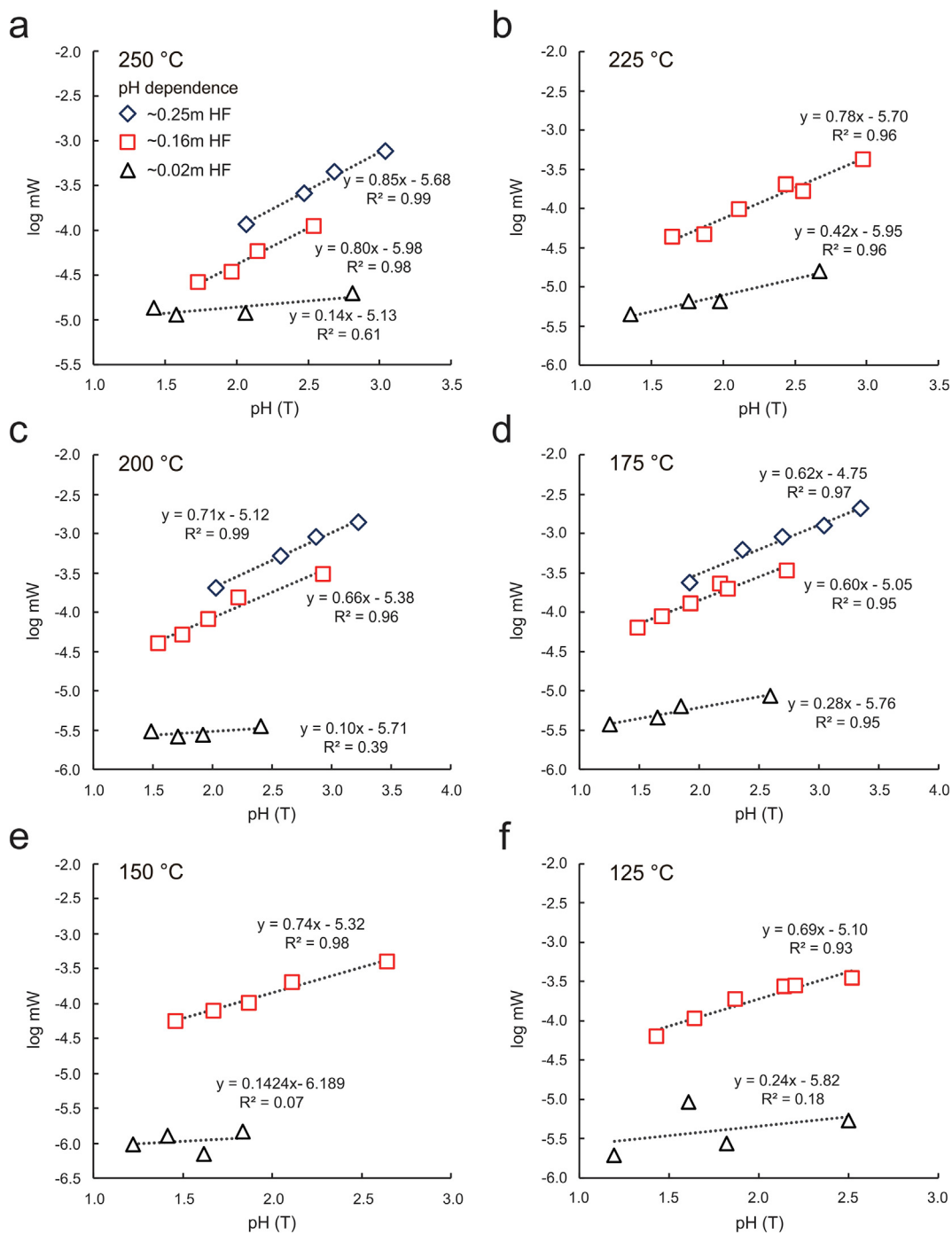


Fig. 4. A plot showing values of $\log m_{\Sigma W}$ at 250 to 125 °C as a function of pH at constant HF molality. The equations “ $y = ax - b$ ” represent linear regressions of the data. A plot for 100 °C is provided in Fig. 4g of Appendix 1.

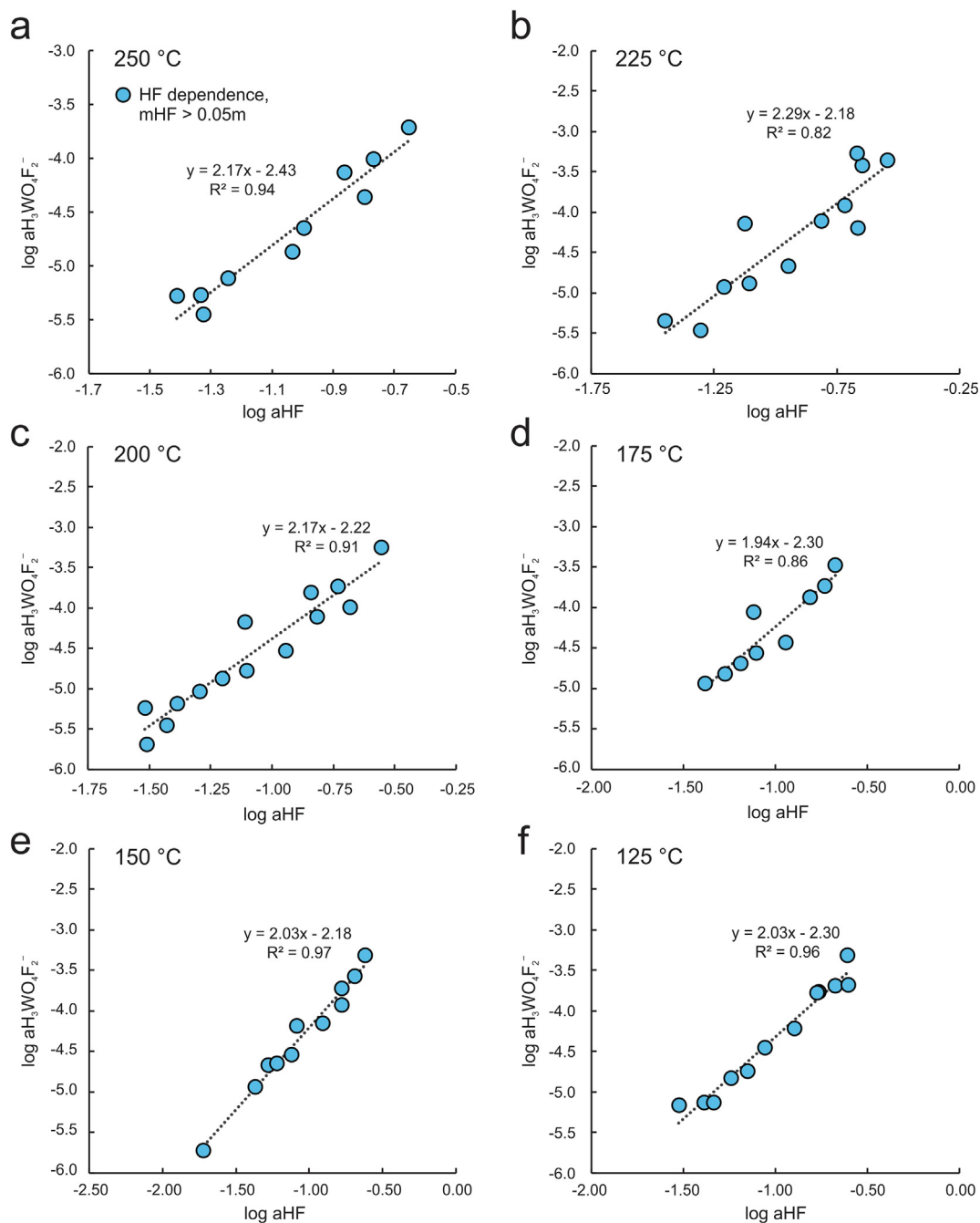


Fig. 5. Plots of $\log a\text{H}_3\text{WO}_4\text{F}_2^-$ versus $\log a\text{HF}$ for a pH of ~ 2 at 250–125 °C. The molality of $\text{H}_3\text{WO}_4\text{F}_2^-$ was calculated by subtracting the concentrations of the tungstate species (H_2WO_4^0 , HWO_4^- and WO_4^{2-}) from the total tungsten concentration. The concentrations of the latter species at the different experimental conditions were calculated using thermodynamic data from Wang et al. (2019) and Shock et al. (1997). The dotted lines represent the linear regressions to the data for $a\text{H}_3\text{WO}_4\text{F}_2^-$ versus $\log a\text{HF}$ at the different temperatures and “ $y = ax - b$ ” the equations of these lines. A plot for 100 °C is provided in Fig. 5g of Appendix 1.

Table 2

Formation constants (log β) for the tungsten species identified in this study based on experiments for temperatures between 100 and 250 °C.

	250 °C	225 °C	200 °C	175 °C	150 °C	125 °C	100 °C
$3\text{H}^+ + \text{WO}_4^{2-} + 2\text{F}^- =$	19.23	18.71	18.17	17.75	17.46	17.11	17.00
$\text{H}_3\text{WO}_4\text{F}_2^-$	± 0.01	± 0.01	± 0.01	± 0.01	± 0.01	± 0.01	± 0.01
$2\text{H}^+ + \text{WO}_4^{2-} = \text{H}_2\text{WO}_4^0$	8.28 ± 0.02	7.98 ± 0.02	7.59 ± 0.02	7.76 ± 0.02	7.07 ± 0.02	7.82 ± 0.02	7.12 ± 0.03

Table 3

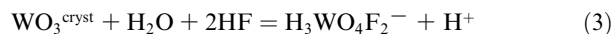
Bryzgalin-Ryzhenko parameters derived for $\text{H}_3\text{WO}_4\text{F}_2^-$ and H_2WO_4^0 based on the formation constants determined in this study.

	pK(298)	A(zz/a)	B(zz/a)
$\text{H}_3\text{WO}_4\text{F}_2^-$	16.981	2.596	218.31
H_2WO_4^0	7.849	1.734	-279.14

concentration. The pH dependency was evaluated with sets of experiments, each of which was conducted with solutions having approximately the same HF concentration.

From Fig. 3, it is evident that the concentration of tungsten was low and roughly constant at low $a\text{HF}$, whereas at higher $a\text{HF}$, $\log m\text{W}$ increased linearly with $\log a\text{HF}$ at a slope between 1.71 and 2.08, suggesting a species with a ligand number of two, i.e., having two fluoride atoms for each tungsten atom. As mentioned above, our earlier study showed that tungsten dissolves mainly as the tungstate species H_2WO_4^0 , HWO_4^- , and WO_4^{2-} in aqueous NaCl-bearing (up to 4 m) solutions at temperatures up to 350 °C (Wang et al., 2019). For comparison to the results of the present study, we calculated the sum of the concentrations of these three species, based on the formation constants for them reported by Wang et al. (2019) and the experimental conditions (e.g., temperature, pH and ionic strength) of the present study. These calculations show that the predicted solubility of the tungstate species (H_2WO_4^0 , HWO_4^- , and WO_4^{2-}) is low and very similar to that measured during the present study for experiments conducted at low $a\text{HF}$ (0.005–0.05 m). They also show that for high $a\text{HF}$ (up to 0.29 m), the solubility of the tungstate species is orders of magnitude lower than that of the species controlling tungsten solubility at elevated HF activity. These observations suggest that at HF concentrations >0.05 m, the dominant tungsten species contains fluorine in a 2:1 ratio with tungsten.

At low $a\text{HF}$ (0.01–0.02 m HF), the tungsten concentration was almost independent of pH; the slope of $\log m\text{W}$ versus pH was consistently <0.5 (Fig. 4), which indicates that tungsten solubility was dominated by the neutral tungstate species, tungstic acid (H_2WO_4^0). In contrast, at high HF concentration (~ 0.16 m to ~ 0.25 m HF), the tungsten concentration ($\log m\text{W}$) increased linearly with pH (the slope varied between 0.60 and 0.85). This correlation of tungsten solubility with pH at high HF concentration and also with $\log a\text{HF}$ (Fig. 3), suggests a major contribution from a tungsten species with a charge of -1 . Given our earlier conclusion that this species contains two fluorine atoms per tungsten atom, we infer that it has the stoichiometry, $\text{H}_3\text{WO}_4\text{F}_2^-$, and that it formed via the reaction:



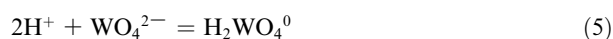
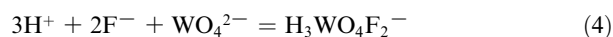
$$\text{Log } K_3 = \log a\text{H}_3\text{WO}_4\text{F}_2^- - \text{pH} - 2\log a\text{HF}$$

The above interpretation is confirmed by the linear dependence of the logarithmic values of the activity of $\text{H}_3\text{WO}_4\text{F}_2^-$ ($\log a\text{H}_3\text{WO}_4\text{F}_2^-$) on $\log a\text{HF}$ at $m\text{HF} > 0.05$ m, and the slope of this dependency, which varies from 1.94 to 2.29 (Fig. 5). The concentration of $\text{H}_3\text{WO}_4\text{F}_2^-$ was calculated assuming that the only tungsten species in the solutions are tungstate species (H_2WO_4^0 , HWO_4^- and WO_4^{2-}) and $\text{H}_3\text{WO}_4\text{F}_2^-$. Thus, the molality of $\text{H}_3\text{WO}_4\text{F}_2^-$ was equal to the total tungsten concentration minus the concentration of tungstate species, which was calculated using the thermodynamic data reported in Wang et al. (2019).

3.2. Evaluation of formation constants (β)

As discussed earlier, the standard Gibbs free energy for $\text{H}_3\text{WO}_4\text{F}_2^-$ and H_2WO_4^0 were determined from the molality of NaCl, HCl, NaF, and tungsten in each experiment using the program OptimA in the HCh software package (Shvarov, 2015); the molality of HCl was calculated from the starting NaCl concentration and the pH and HF measured after each experiment. In addition to the two tungsten species, the following aqueous species were also considered in the calculations: O_2 , H_2 , H^+ , OH^- , Na^+ , Cl^- , F^- , NaOH^0 , NaCl^0 , NaF^0 , HCl^0 , HF^0 , HWO_4^- and WO_4^{2-} . Thermodynamic data for these species were obtained from Johnson et al. (1992), Shock et al. (1997), Sverjensky et al. (1997) and Wang et al. (2019) and values for the extended parameter for NaCl were taken from Oelkers and Helgeson (1991). Thermodynamic data for the tungsten and molybdenum oxide solids (WO_3 , MoO_2 and MoO_3) were taken from Pankratz and Mrazek (1982) and Robie and Hemingway (1995). The sources of these data are listed in the Appendix 2.

With the standard Gibbs free energy of $\text{H}_3\text{WO}_4\text{F}_2^-$ and H_2WO_4^0 in hand, the Gibbs free energy changes for the reactions responsible for the formation of these species were calculated using the standard Gibbs free energy of the other species involved in the reactions, namely WO_4^{2-} , F^- , and H^+ .



Thermodynamic data for WO_4^{2-} and F^- were taken from Shock et al. (1997). The formation constants ($\log \beta$) were calculated using the relationship $\Delta G^\circ = -RT \ln K$. These formation constants and the uncertainty associated with their determination are reported in Table 2; the

Table 4

Logarithms of equilibrium constants ($\log K$) and their associated uncertainty for the $\text{WO}_3^{\text{cryst}}$ dissolution reactions.

	250 °C	225 °C	200 °C	175 °C	150 °C	125 °C	100 °C
$\text{WO}_3^{\text{cryst}} + \text{H}_2\text{O}$	-5.10	-4.93	-4.77	-4.63	-4.51	-4.43	-4.39
$+ 2\text{HF} = \text{H}_3\text{WO}_4\text{F}_2^- + \text{H}^+$	± 0.17	± 0.13	± 0.16	± 0.14	± 0.12	± 0.13	± 0.18
$\text{WO}_3^{\text{cryst}} + \text{H}_2\text{O} = \text{H}_2\text{WO}_4^0$	-5.20	-5.33	-5.48	-5.65	-5.85	-6.07	-6.34
	± 0.22	± 0.10	± 0.10	± 0.33	± 0.19	± 0.56	± 0.21

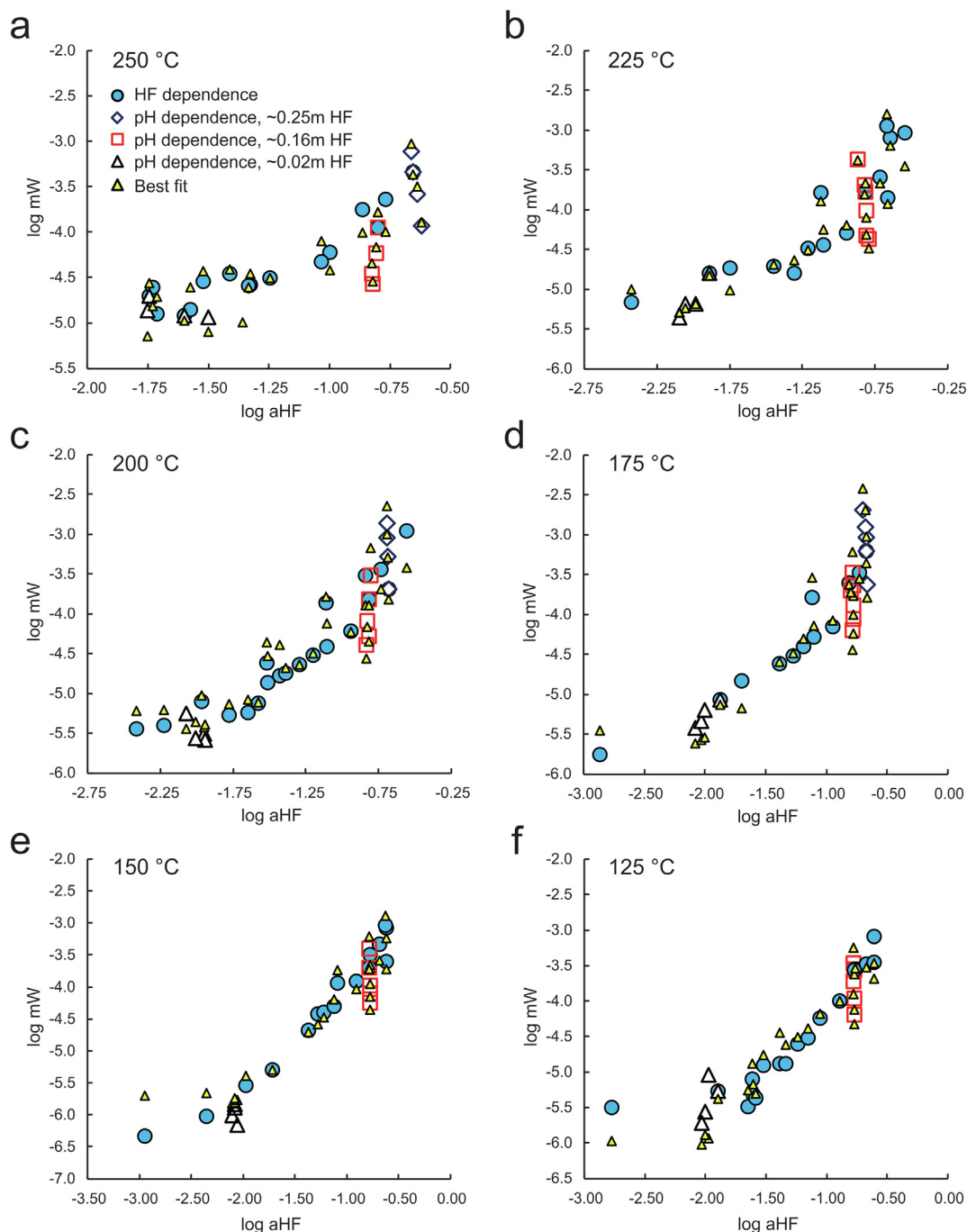


Fig. 6. Plots of $\log m\Sigma W$ versus $\log a_{HF}$ comparing the results of the experiments conducted in this study with the predicted $\log m\Sigma W$ values for the same conditions calculated using $\log K$ values retrieved from these data at 250 to 125 °C. The symbols are the same as those used in Figs. 3 and 4, and illustrate the dependence of tungsten concentration on HF activity and pH, respectively. A plot for 100 °C is provided in Fig. 6g of Appendix 1.

uncertainty was calculated using the OptimA program. The formation constants for $H_3WO_4F_2^-$ and $H_2WO_4^0$ at the different temperatures were fitted to the Bryzgalin-Ryzhenko model (Ryzhenko et al., 1985) modified by Shvarov and Bastrakov (1999):

$$\log K_{(T,P)} = \frac{T_r}{T} \log K_{(T_r,P_r)} + B_{(T,P)} \left(A_{zz/a} + \frac{B_{zz/a}}{T} \right) \quad (6)$$

In this equation, K is the formation constant for the species of interest, T_r , P_r are the reference temperature and pressure, and $A_{zz/a}$ and $B_{zz/a}$ are fitting parameters (Table 3). The term $B_{(T,P)}$ was computed from the dissociation constant of water (Marshall and Franck, 1981) at temperature T and pressure P . The formation constants so calculated were used to calculate equilibrium constants ($\log K$) for the tungsten oxide dissolution reactions. These values are

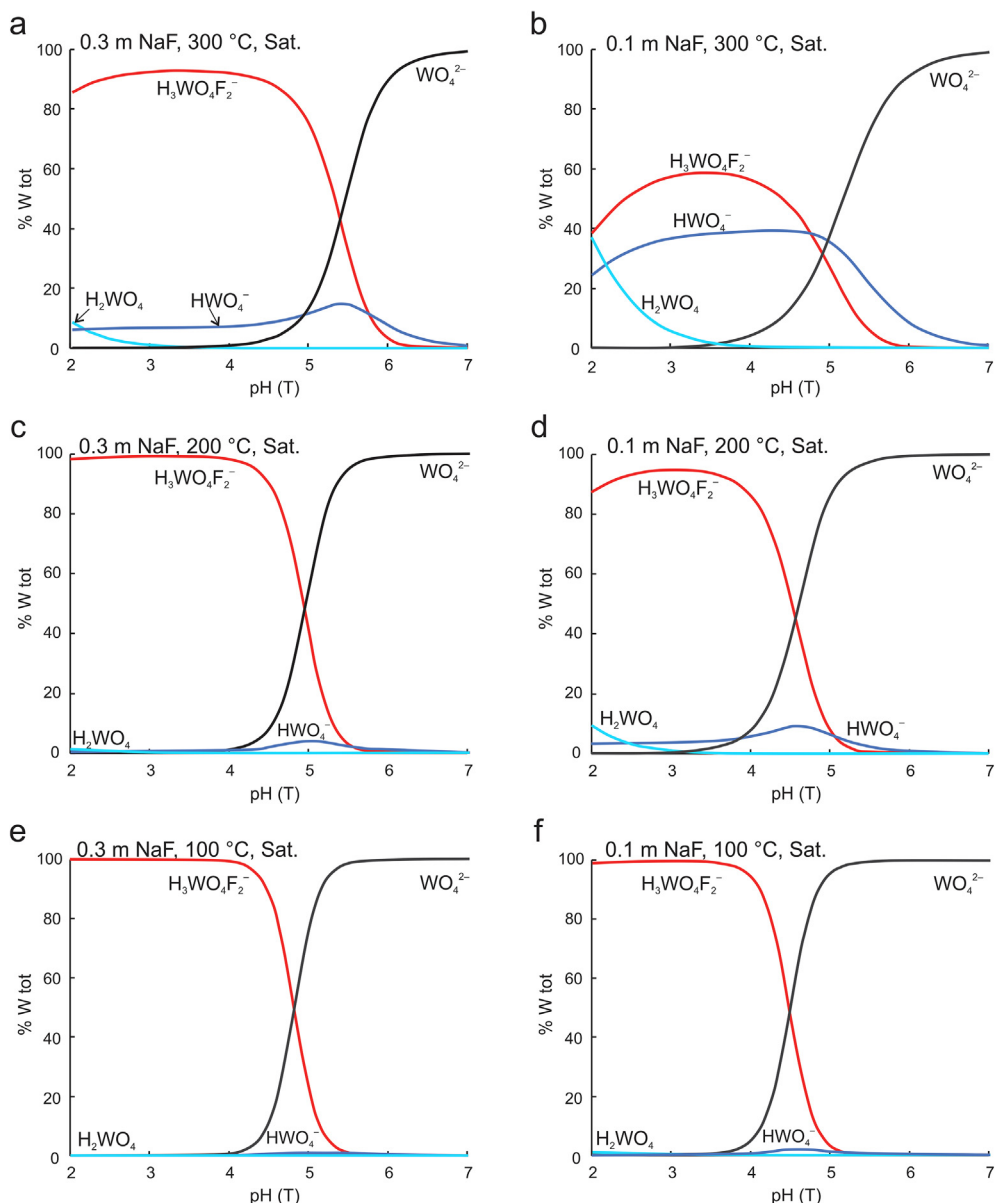


Fig. 7. Proportions of $\text{H}_3\text{WO}_4\text{F}_2^-$, H_2WO_4^0 , HWO_4^- , and WO_4^{2-} in aqueous fluids containing 1.8 m NaCl and 0.3 m NaF (a), (c), (e) and 0.1 m NaF (b), (d), (f) as a function of pH at 300, 200, and 100 °C, and saturated vapor pressure, based on the results of this study. The thermodynamic data for H_2WO_4^0 and HWO_4^- are from Wang et al. (2019), and for WO_4^{2-} are from Shock et al. (1997).

reported in Table 4. Uncertainties in the equilibrium constants were determined by calculating the log K values for each data point using the tungsten activity, mHF, pH(T), and Reactions (3) and (7), and then calculating the standard deviation of these values, at each temperature.



$$\text{Log } K_7 = \text{log } a_{\text{H}_2\text{WO}_4^0} \quad 40$$

Finally, the thermodynamic data retrieved in this study were used to fit the experimental data (Fig. 6). The results show that the thermodynamically calculated tungsten concentrations agree very well with those determined experimentally.

4. DISCUSSION

4.1. Dominant tungsten species in fluoride-bearing solutions

In our previous study, we showed that HWO_4^- and WO_4^{2-} are the dominant tungsten species in aqueous solutions at temperatures up to 350 °C at near-neutral and alkaline conditions, respectively, and that tungstic acid is the dominant species at low pH (Wang et al., 2019). We also showed that this is the case, even at high salinity (up to 4 m NaCl). In contrast, we have demonstrated in the present study that, in the presence of HF, tungsten oxide dissolves to form the species $\text{H}_3\text{WO}_4\text{F}_2^-$ and that, at high HF concentration and low pH (<3.4), this is the dominant

Table 5

The compositions of the fluids and granite employed in modeling fluid-rock interaction.

Magmatic fluid ^a (300 °C and 500 bar)						Granite ^b	
Fluorine-bearing			Fluorine-free			Major elements (wt.%)	
	mol/kg	wt.% or ppm		mol/kg	wt.% or ppm	SiO ₂	74.97
NaCl	1.8 m	~10 wt.%	NaCl	1.8 m	~10 wt.%	Al ₂ O ₃	13.43
NaF	0.15 m	2850 ppm (∑F)	NaF	0 m	0 ppm (∑F)	Fe ₂ O ₃ ^T	1.58
CaCl ₂	0.01 m	400 ppm (∑Ca)	CaCl ₂	0.01 m	400 ppm (∑Ca)	CaO	0.75
FeCl ₂	0.0005 m	28 ppm (∑Fe)	FeCl ₂	0.0005 m	28 ppm (∑Fe)	Na ₂ O	3.58
H ₂ S	0.016 m	512 ppm (∑S)	H ₂ S	0.016 m	512 ppm (∑S)	K ₂ O	4.64
KCl	0.2 m	7800 ppm (∑K)	KCl	0.2 m	7800 ppm (∑K)	MgO	0.13
MgCl ₂	0.02 m	486 ppm (∑Mg)	MgCl ₂	0.02 m	486 ppm (∑Mg)	Total	99.08
As ₂ O ₃	0.0015 m	225 ppm (∑As)	As ₂ O ₃	0.0015 m	225 ppm (∑As)	Mineral composition (g)	
HCl	0.1376 m		HCl	0.0001 m		Microcline	244
pH(T) ^c	3.00		pH(T) ^c	3.00		Albite	303
∑W ^c	0.000135 m	24.8 ppm	∑W ^c	0.000012 m	2.2 ppm	Anorthite	37
∑Si ^c	0.025 m	715 ppm	∑Si ^c	0.0082 m	230 ppm	Annite	45
						Quartz	367
						Phlogopite	4
						Total	1000

Note:

^a The composition of the magmatic hydrothermal fluid is based on the compositions of fluid inclusions from granite-related tungsten deposits (Lecumberri-Sanchez et al., 2017; Yang et al., 2019; Pan et al., 2019).

^b The composition of the granite is that of garnet-bearing porphyritic fine-grained biotite granite from the Xihuashan deposit, a typical granite-hosted vein-type tungsten deposit in China (Guo et al., 2012). The mineral composition of the granite was calculated from the its major element composition using the relationship $X = B/A$ where X is a vector of the proportions of the different minerals, B is a matrix of mineral compositions and A is a vector corresponding to the bulk rock chemical composition. The formulae and sources of thermodynamic data for the minerals are listed in Appendix 2.

^c The concentrations of W and Si in the fluid corresponded to saturation with WO_3^{ctyst} and quartz; the pH(T) represents the pH value of the fluid after saturation at 300 °C.

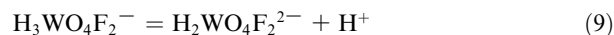
tungsten species in aqueous solutions at temperatures between 100 and 250 °C. To integrate the results of our two studies, noting that tungsten speciation is highly dependent on pH, we used the thermodynamic data retrieved in them to evaluate tungsten speciation as a function of pH for temperatures up to 300 °C. We did so by modeling the dissolution of tungsten trioxide in aqueous fluids containing 1.8 m NaCl and 0.1 and 0.3 m NaF. The thermodynamic data for $H_3WO_4F_2^-$ and $H_2WO_4^0$ are from this study, those for HWO_4^- are from Wang et al. (2019) and for WO_4^{2-} are from Shock et al. (1997).

The results of this modeling show that $H_3WO_4F_2^-$ is the dominant tungsten species for pH values lower than ~5, and that the species WO_4^{2-} is dominant at higher pH, except at 300 °C in fluids containing 0.1 m HF (Fig. 7). For this exception, HWO_4^- predominates at near-neutral pH. The contribution of HWO_4^- to tungsten solubility, however, decreases with decreasing temperature (and increasing HF activity) and at 100 °C is insignificant. The importance of $H_3WO_4F_2^-$ increases with increasing HF activity (and decreasing pH) as predicted by Reaction (8).



Although our evaluation of tungsten speciation reached the conclusion that $H_3WO_4F_2^-$ is the dominant tungsten species at pH values below 5 and that the tungstate ion (WO_4^{2-}) predominates at higher pH, this does not rule out the possibility that other fluoride-bearing tungsten species, not detected by us because of the acidic conditions of our

experiments, may be important for tungsten transport at high pH. Indeed, it is reasonable to predict that the species $H_3WO_4F_2^-$ will dissociate with progressively higher pH to yield the species $H_2WO_4F_2^{2-}$, $HWO_4F_2^{3-}$ and $WO_4F_2^{4-}$ via reactions of the type:



Whether these species could play a role in the transport of tungsten at high pH, however, needs to be the subject of further experimental study.

4.2. Implications for ore genesis

The global tungsten resource is dominated by two major classes of deposits, namely the vein and greisen classes, in which the principal ore mineral is wolframite, and the skarn class in which the tungsten occurs mainly as scheelite (Polya, 1989; Lu et al., 2003; Hu and Zhou, 2012; Lecumberri-Sanchez et al., 2017; Soloviev and Kryazhev, 2017; Pan et al., 2019). Both classes, however, are closely associated with highly fractionated, fluorine-rich (0.22–0.99 wt.%) peraluminous ($A/CNK = 1.05–1.16$) granites (Polya, 1989; Lu et al., 2003; Wu et al., 2017). The mineralization occurs either within the granite (vein- and greisen-type) or in contact metamorphic rocks adjacent to the granite (both types; skarn where the rocks are calcareous) and is interpreted to be the product of hydrothermal fluids exsolved from the corresponding magma (Polya, 1989; Wood and Samson, 2000; Lecumberri-Sanchez et al.,

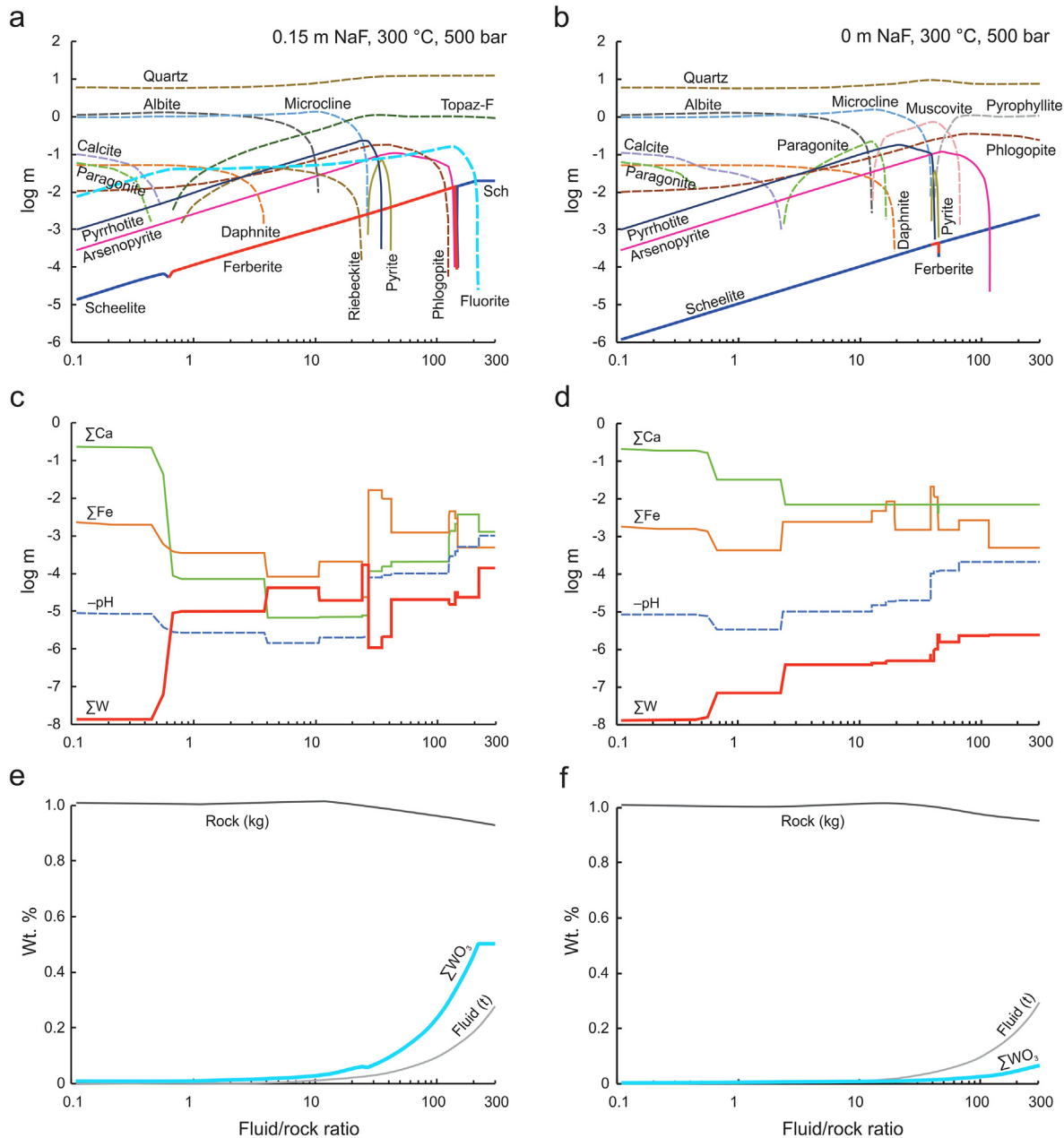


Fig. 8. Models of the reaction of fluorine-bearing and fluorine-free magmatic hydrothermal fluids with 1 Kg of granite at 300 °C, $f_{O_2} = FMQ + 1$, $X_{CO_2} = 0.01$, and 500 bar, as a function of the fluid/rock ratio. a) and b) Changes in the moles of minerals per kilogram of rock (log m) with fluid/rock ratio for a fluorine-bearing (0.15 m HF) and fluorine-free fluid, respectively. Sch is the abbreviation of scheelite. c) and d) Changes in the total concentrations of Ca, Fe and W and the pH with fluid/rock ratio for the fluorine-bearing (0.15 m HF) and fluorine-free fluid, respectively. (e) and (f) The total concentration of WO_3 with fluid/rock ratio for the fluorine-bearing (0.15 m HF) and fluorine-free fluid, respectively. The terms Rock (kg) and Fluid (t) refer to the mass of rock and fluid in the system in units of kilogram and ton, respectively and log m to log mole. The fluids were introduced in 100 g aliquots. Their initial compositions and that of the granite are reported in Table 5.

2017). An important observation, in the context of the current study, is that alteration accompanying the tungsten mineralization is commonly characterized by the occurrence of topaz, fluorite and fluorine-bearing mica (these minerals may also be part of the vein gangue assemblage). This implies that, like the granites, the ore fluids are enriched in fluorine. Although previous studies have not reported the fluoride concentration of the ore-forming fluids, this concentration can be estimated from the coefficient

for the partitioning of fluoride between fluid and melt and the fluorine content of the latter. Based on the experiments of Webster (1990), the partition coefficient of fluoride between an aqueous fluid and a peraluminous granitic melt containing up to ~1 wt.% fluorine (see above) is 0.15–0.37 at 800–1000 °C and 2 kbar. Thus, the fluorine concentration of the ore-forming fluid for a tungsten deposit is predicted to be in the range of 330–3700 ppm (0.02–0.19 m). This prediction is consistent with direct measurements by

Vasyukova and Williams-Jones (2018) of the fluoride concentration of fluid inclusions (780–6509 ppm; 0.04–0.33 m) in a highly fractionated granite.

Microthermometric measurements of phase changes in primary fluid inclusions in scheelite and wolframite, the principal tungsten ore minerals for a variety of tungsten deposits, indicate that these ore minerals precipitate at a temperature of 250–350 °C from aqueous-carbonic fluids containing between 3 and 12 wt.% NaCl equivalent (Campbell and Robinsoncook, 1987; Polyá, 1989; Bailly et al., 2002; Lu et al., 2003; Wei et al., 2012; Ni et al., 2015; Lecumberri-Sanchez et al., 2017; Pan et al., 2019). The dominant carbonic species is CO₂ and occurs in mole fractions (X_{CO_2}) ranging from less than 0.01 to 0.1 (Wood and Samson, 2000; Wei et al., 2012; Pan et al., 2019). The oxygen fugacity of the ore-forming fluid is thought to lie mostly between that of the fayalite-magnetite-quartz (FMQ) and Ni-NiO (NNO) buffers, and the pH to be between 3 and 6 (Polyá, 1989; Wood and Samson, 2000). Thus, based on our earlier discussion, the dominant tungsten species in the ore-forming fluid, the pH of which is predicted to be less than the pH of the assemblage muscovite-K-feldspar-quartz (~5), a commonly observed alteration assemblage in granite-related tungsten deposits, is H₃WO₄-F₂⁻. Finally, in-situ studies of the composition of fluid inclusions in quartz of ore from greisen and quartz-vein type tungsten deposits indicate that the ore-forming fluid contains variable concentrations of K (338–7453 ppm; 0.0087–0.19 m), Al (32–4010 ppm; 0.0012–0.15 m), Mg (0.3–271 ppm; 0.000013–0.011 m), As (4.4–582 ppm; 0.0001–0.0078 m), W (0.3–169 ppm; 0–0.00092 m), Fe (0–52 ppm; 0–0.00093 m), Ca (0–452 ppm; 0–0.011 m), and S (0–3663 ppm; 0–0.12 m) (Lecumberri-Sanchez et al., 2017; Yang et al., 2019; Pan et al., 2019).

There is still no consensus on the genesis of granite-related tungsten deposits, other than that they are products of magmatic hydrothermal fluids, with opinion being divided over whether ore deposition is due to fluid mixing, boiling or fluid-rock interaction (Campbell and Robinsoncook, 1987; Polyá, 1989; Heinrich, 1990; Lu et al., 2003; Wei et al., 2012; Ni et al., 2015; Lecumberri-Sanchez et al., 2017; Pan et al., 2019). The study of Lecumberri-Sanchez et al. (2017), however, has made a convincing case that, whereas the tungsten is transported by the ore fluid, the Ca and Fe necessary for deposition of the scheelite and wolframite ores are supplied by the host rock during its interaction with this fluid. Here, we build on the results of that study by quantitatively evaluating the interaction of a relatively fluoride-rich, tungsten-bearing magmatic hydrothermal fluid with a granite and the role of this interaction in the deposition of scheelite (CaWO₄) and wolframite ((Mn, Fe)WO₄) ores. For simplicity, ferberite (FeWO₄) was taken to represent wolframite. Thermodynamic data for the minerals and aqueous species were obtained from Johnson et al. (1992), Robie and Hemingway (1995), Shock et al. (1997), Sverjensky et al. (1997), Tagirov et al. (1997), Wood and Samson (2000), Pokrovski et al. (2002), Testemale et al. (2009), Holland and Powell (2011), and Wang et al. (2019). These data are reported in Appendix 2.

The interaction of granite with a magmatic hydrothermal ore fluid containing 0.15 m NaF (2850 ppm ΣF), which is within the range of fluorine concentrations observed in magmatic hydrothermal fluids, was modeled for 300 °C, $f_{O_2} = FMQ + 1$, $X_{CO_2} = 0.01$, and 500 bar using the HCh software of Shvarov (2008). This involved equilibrating 1 kg of granite with a 100 g aliquot of the ore fluid, removing the fluid, reacting the altered granite with a second 100 g aliquot of ore fluid, removing it and continuing the process until a fluid/rock ratio of 300 was achieved. The fluid contained 1.8 m NaCl (~10 wt.%), 0.2 m KCl, 0.02 m MgCl₂, 0.016 m H₂S, 0.01 m CaCl₂, 0.0005 m FeCl₂, 0.0015 m As₂O₃ and was saturated with quartz (Table 5). It thus has a composition similar to the magmatic-hydrothermal fluid inclusions from granite-related deposits discussed in Lecumberri-Sanchez et al. (2017), Pan et al. (2019) and Yang et al. (2019). The tungsten concentration of the ore fluid (24.8 ppm or 0.000135 m) corresponded to saturation of the fluid with WO₃^{cryst} and is within the range of values mentioned above for fluid inclusions from greisen and vein-type tungsten deposits. The composition of the granite was taken to be that of garnet-bearing porphyritic fine-grained biotite granite from the Xihuashan deposit, a typical granite-hosted vein-type tungsten deposit in China (Table 5; Guo et al., 2012), which is a highly fractionated granite similar to those associated with tungsten deposits elsewhere (Campbell and Robinsoncook, 1987; Polyá, 1989; Lu et al., 2003; Wu et al., 2017; Soloviev and Kryazhev, 2017; Song et al., 2018). The initial pH was 3, which is the probable lower limit of the pH of a tungsten ore fluid (Wood and Samson, 2000). For comparison, the granite was also allowed to interact with a fluorine-free equivalent of the above fluid (Table 5).

The results of the modeling are presented in Fig. 8 as a function of the fluid/rock ratio. They show that interaction of granite with the fluorine-bearing fluid leads to the progressive replacement of the major rock-forming minerals, microcline and albite, by topaz and to a lesser extent fluorite, with increasing fluid/rock ratio (Fig. 8a). This alteration is accompanied initially by deposition of minor amounts of scheelite, which is replaced by ferberite at a fluid/rock ratio of 0.6 and, in turn, by scheelite at a fluid/rock ratio in excess of 140. The pH climbs immediately from the initial value of 3 to a value of ~5 and then gradually in steps to a value of ~6 (Fig. 8c). The concentration of W increases sharply between a fluid/rock ratio of 0.5 and 0.6, which corresponds to a sharp drop in the concentration of Ca due to the crystallization of fluorite, and a resulting suppression in the crystallization of scheelite (Fig. 8c). At higher fluid/rock ratios, the increase in W concentration is more gradual, due to ferberite deposition and a reduction in the rate of decrease of Fe concentration. The latter also promoted precipitation of arsenopyrite, a mineral that saturated at the onset of fluid-rock interaction and is commonly associated with wolframite in granite-related tungsten deposits (Polyá, 1989; Lu et al., 2003; Wei et al., 2012; Soloviev and Kryazhev, 2017; Pan et al., 2019). The Ca concentration, however, continues to fall as a result of the ongoing crystallization of fluorite, thereby explaining the continued deposition of ferberite. At a fluid/rock ratio

of ~ 27 , there is an abrupt increase in the concentration of Fe, which reflects the exhaustion of feldspar and decreasing of the pH of fluid and the consequent termination of pyrrhotite precipitation. This enabled the further deposition of both ferberite and arsenopyrite. Although the Ca concentration also starts increasing at this fluid/rock ratio, it remains at a much lower absolute level than that of Fe, ensuring further deposition of ferberite as the only tungsten mineral. Indeed, it is only after the mass of fluorite precipitated reaches a maximum at a fluid/rock ratio of ~ 140 and begins to decrease that scheelite reappears as a late saturating phase.

Although interaction of the fluorine-free with granite also leads to a progressive replacement of the major rock-forming minerals, microcline and albite, with increasing fluid/rock ratio, this replacement is by paragonite, muscovite and pyrophyllite rather than by topaz and fluorite (Fig. 8b). Moreover, whereas ferberite deposits over a wide interval of fluid/rock ratio from the fluorine-bearing fluid, scheelite is the only tungsten mineral to deposit from the fluorine-free fluid, except for a very narrow interval of fluid/rock ratios (38–44), over which it is replaced by ferberite. The amount of scheelite precipitated at any fluid/rock ratio is also much less than that of ferberite at the same fluid/rock ratio from the fluorine-bearing fluid. This difference in behavior is due to the fact that in the absence of fluorite crystallization, for fluid/rock ratios above 0.6, the concentration of Ca in the fluorine-free fluid is consistently higher than in the fluorine-bearing fluid (Fig. 8d). Indeed, the Ca concentration of the fluorine-free fluid is nearly three orders of magnitude higher than that of the fluorine-bearing fluid at fluid/rock ratios between 4 and 27, and at a fluid/rock ratio of 100 it is one order of magnitude higher. Although the Fe concentration is also higher in the fluorine-free fluid than in the fluorine-bearing fluid for a wide range of fluid/rock ratios, it is almost invariably lower than that of Ca.

In addition to not precipitating ferberite, the fluorine-free fluid deposited approximately 10% of the mass of WO_3 deposited by the fluorine-bearing fluid for the same fluid/rock ratio and at no reasonable fluid/rock ratio was able to achieve an economic concentration of WO_3 (Fig. 8e and f). In contrast the grade of WO_3 deposited by the fluorine-bearing fluid for a fluid/rock ratio of 45 was 0.1 wt%, which is within the range of grades reported for large granite-hosted tungsten deposits exploited by open pit mining methods (Schmidt et al., 2012). To summarize, scheelite was the only tungsten mineral deposited by the fluorine-free fluid, except for a very narrow interval of fluid/rock ratios, because of the high Ca/Fe ratio of the fluid, whereas the very low Ca/Fe ratio for a wide range of fluid/rock ratios, due to the precipitation of fluorite, ensured that ferberite was the main ore mineral deposited by the fluorine-bearing fluid. Our modeling illustrates the central role played by fluorine in determining the grade and ore mineralogy of granite-hosted vein- and greisen-type tungsten deposits and shows convincingly that the high solubility of tungsten as $\text{H}_3\text{WO}_4\text{F}_2^-$ and early fluorite saturation are the major reasons why these deposits are economi-

cally viable and contain wolframite as their principal ore mineral.

5. CONCLUSIONS

The results of this study show that tungsten is dissolved in HF-bearing fluids dominantly as $\text{H}_3\text{WO}_4\text{F}_2^-$ at acidic to near-neutral pH and suggest that tungstate fluoride species, such as $\text{H}_2\text{WO}_4\text{F}_2^{2-}$, may be important at higher pH. A model employing these results showed that, owing to the formation of $\text{H}_3\text{WO}_4\text{F}_2^-$, ten times as much tungsten is deposited from a fluorine-bearing ore fluid (0.15 m HF) during granite-fluid interaction than from an otherwise identical fluorine-free fluid. Finally, the study showed that saturation of the ore fluid with fluorite is an essential trigger for tungsten mineralization in granites and the reason that the ores are dominated by wolframite rather than scheelite.

Declaration of Competing Interest

The authors declare that they have no known competing financial interests or personal relationships that could have appeared to influence the work reported in this paper.

ACKNOWLEDGEMENTS

The experimental work described in this paper was carried out in the Fluid-Rock Interaction Laboratory, Department of Earth and Planetary Sciences, McGill University and was funded by the Strategic Priority Research Program (B) of the Chinese Academy of Sciences (XDB18000000), a NSERC Discovery grant to AEW-J, grants from the National Natural Science Foundation of China (41603052; 41673067), the national Key R&D Program of China (2016YFC0600503), and an Open Research Fund of the State Key Laboratory of Ore Deposit Geochemistry to AEW-J. We thank Artaches Migdisov, Alexander Timofeev, and Yuan Mei for discussions that helped improve the manuscript, Anna Katharina Jung and Longbo Yang for their assistance in conducting the ICP-MS analyses, and Yong Meng for his assistance in performing the XRD analyses. The constructive reviews of Matthew Steele-MacInnis and two anonymous referees helped improve the manuscript, as did the editorial assistance and comments of Associate Editor Martin Reich.

APPENDIX A. SUPPLEMENTARY MATERIAL

Supplementary data to this article can be found online at <https://doi.org/10.1016/j.gca.2020.09.032>.

REFERENCES

- Bailly L., Grancea L. and Kouzmanov K. (2002) Infrared microthermometry and chemistry of wolframite from the Baia Sprie epithermal deposit, Romania. *Econ. Geol.* **97**, 415–423.
- Campbell A. R. and Robinsoncook S. (1987) Infrared fluid inclusion microthermometry on coexisting wolframite and quartz. *Econ. Geol.* **82**, 1640–1645.
- Guo C. L., Chen Y. C., Zeng Z. L. and Lou F. S. (2012) Petrogenesis of the Xihuashan granites in southeastern China: constraints from geochemistry and in-situ analyses of zircon U-Pb-Hf-O isotopes. *Lithos* **148**, 209–227.

- Hayes S. M. and McCullough E. A. (2018) Critical minerals: a review of elemental trends in comprehensive criticality studies. *Resour. Policy* **59**, 192–199.
- Heinrich C. A. (1990) The chemistry of hydrothermal tin-tungsten ore deposition. *Econ. Geol.* **85**, 457–481.
- Helgeson H. C. and Kirkham D. H. (1974) Theoretical prediction of the thermodynamic behavior of aqueous electrolytes at high pressures and temperatures; I, Summary of the thermodynamic/electrostatic properties of the solvent. *Am. J. Sci.* **274**, 1089–1198.
- Helgeson H. C., Kirkham D. H. and Flowers G. C. (1981) Theoretical prediction of the thermodynamic behavior of aqueous electrolytes by high pressures and temperatures; IV, Calculation of activity coefficients, osmotic coefficients, and apparent molal and standard and relative partial molal properties to 600 degrees C and 5kb. *Am. J. Sci.* **281**, 1249–1516.
- Holland T. J. B. and Powell R. (2011) An improved and extended internally consistent thermodynamic dataset for phases of petrological interest, involving a new equation of state for solids. *J. Metamorph. Geol.* **29**, 333–383.
- Hu R.-Z. and Zhou M.-F. (2012) Multiple Mesozoic mineralization events in South China—an introduction to the thematic issue. *Miner. Depos.* **47**, 579–588.
- Johnson J. W., Oelkers E. H. and Helgeson H. C. (1992) SUPCRT92: a software package for calculating the standard molal thermodynamic properties of minerals, gases, aqueous species, and reactions from 1 to 5000 bar and 0 to 1000°C. *Comput. Geosci.* **18**, 899–947.
- Keppeler H. and Wyllie P. J. (1991) Partitioning of Cu, Sn, Mo, W, U, and Th between melt and aqueous fluid in the systems haplogranite-H₂O-HCl and haplogranite-H₂O-HF. *Contrib. Mineral. Petrol.* **109**, 139–150.
- Kestin J., Sengers J. V., Kamgar-Parsi B. and Sengers J. M. H. L. (1984) Thermophysical properties of fluid H₂O. *J. Phys. Chem. Ref. Data* **13**, 175–183.
- Lecumberri-Sanchez P., Vieira R., Heinrich C. A., Pinto F. and Walle M. (2017) Fluid-rock interaction is decisive for the formation of tungsten deposits. *Geology* **45**, 579–582.
- Liu Y. J. and Ma D. S. (1987) *Geochemistry of Tungsten*. Science press, Beijing (in Chinese).
- Lu H. Z., Liu Y. M., Wang C. L., Xu Y. Z. and Li H. Q. (2003) Mineralization and fluid inclusion study of the Shizhuyuan W-Sn-Bi-Mo-F skarn deposit, Hunan province, Cehina. *Econ. Geol.* **98**, 955–974.
- Manning D. A. C. and Henderson P. (1984) The behavior of tungsten in granitic melt-vapor systems. *Contrib. Mineral. Petrol.* **86**, 286–293.
- Marshall W. L. and Franck E. U. (1981) Ion product of water substance, 0–1000 °C, 1–10,000 bars new international formulation and its background. *J. Phys. Chem. Ref. Data* **10**, 295–304.
- Migdisov A. A. and Williams-Jones A. E. (2007) An experimental study of the solubility and speciation of neodymium (III) fluoride in F-bearing aqueous solutions. *Geochim. Cosmochim. Acta* **71**, 3056–3069.
- Ni P., Wang X.-D., Wang G.-G., Huang J.-B., Pan J.-Y. and Wang T.-G. (2015) An infrared microthermometric study of fluid inclusions in coexisting quartz and wolframite from Late Mesozoic tungsten deposits in the Gannan metallogenic belt, South China. *Ore Geol. Rev.* **65**, 1062–1077.
- Oelkers E. H. and Helgeson H. C. (1990) Triple-ion anions and polynuclear complexing in supercritical electrolyte solutions. *Geochim. Cosmochim. Acta* **54**, 727–738.
- Oelkers E. H. and Helgeson H. C. (1991) Calculation of activity coefficients and degrees of formation of neutral ion pairs in supercritical electrolyte solutions. *Geochim. Cosmochim. Acta* **55**, 1235–1251.
- Pan J. Y., Ni P. and Wang R. C. (2019) Comparison of fluid processes in coexisting wolframite and quartz from a giant vein-type tungsten deposit, South China: insights from detailed petrography and LA-ICP-MS analysis of fluid inclusions. *Am. Miner.* **104**, 1092–1116.
- Pankratz L. and Mrazek R. V. (1982) Thermodynamic properties of elements and oxides. U.S. Bureau of Mines Bulletin, 672.
- Polya D. A. (1989) Chemistry of the main-stage ore-forming fluids of the Panasqueira W-Cu(Ag)-Sn deposit, Portugal - implications for models of ore genesis. *Econ. Geol.* **84**, 1134–1152.
- Pokrovski G. S., Kara S. and Roux J. (2002) Stability and solubility of arsenopyrite, FeAsS, in crustal fluids. *Geochim. Cosmochim. Acta* **66**, 2361–2378.
- Robie R. A. and Hemingway B. S. (1995) Thermodynamic properties of minerals and related substances at 298.15 K and 1 bar (105 pascals) pressure and at higher temperatures.
- Romer R. L. and Lüders V. (2006) Direct dating of hydrothermal W mineralization: U-Pb age for hüberite (MnWO₄), Sweet Home Mine, Colorado. *Geochim. Cosmochim. Acta* **70**, 4725–4733.
- Ryzhenko B. N., Bryzgalin O. V., Artamkina I. Y., Spasennykh M. Y. and Shapkin A. I. (1985) An electrostatic model for the electrolytic dissociation of inorganic substances dissolved in water. *Geochem. Int.* **22**, 128–144.
- Schmidt S., Berghau W. and Hutten A. (2012) From deposit to concentrate: the basics of tungsten mining Part 1: Project generation and project development. *Int. Tungsten Ind. Assoc.* **4**, 1–20.
- Schröcke H., Trumm A. and Hochleitner R. (1984) Über den transport von Wolfram und den Absatz von Wolfram-Doppel-Oxiden in fluiden wässrigen Lösungen. *Geochim. Cosmochim. Acta* **48**, 1791–1805.
- Shock E. L., Sassani D. C., Willis M. and Sverjensky D. A. (1997) Inorganic species in geologic fluids: correlations among standard molal thermodynamic properties of aqueous ions and hydroxide complexes. *Geochim. Cosmochim. Acta* **61**, 907–950.
- Shvarov Y. (2015) A suite of programs, OptimA, OptimB, OptimC, and OptimS compatible with the Unitherm database, for deriving the thermodynamic properties of aqueous species from solubility, potentiometry and spectroscopy measurements. *Appl. Geochem.* **55**, 17–27.
- Shvarov Y. V. and Bastrakov E. (1999) HCh: a software package for geochemical equilibrium modelling. *User's Guide* **25**.
- Shvarov Y. V. (2008) HCh: New potentialities for the thermodynamic simulation of geochemical systems offered by windows. *Geochem. Int.* **46**, 834–839.
- Sverjensky D. A., Shock E. L. and Helgeson H. C. (1997) Prediction of the thermodynamic properties of aqueous metal complexes to 1000°C and 5 kb. *Geochim. Cosmochim. Acta* **61**, 1359–1412.
- Soloviev S. G. and Kryazhev S. G. (2017) Geology, mineralization, and fluid inclusion characteristics of the Skrytoe reduced-type W skarn and stockwork deposit, Sikhote-Alin, Russia. *Miner. Depos.* **52**, 903–928.
- Song W. L., Yao J. M., Chen H. Y., Sun W. D., Ding J. Y., Xiang X. K., Zuo Q. S. and Lai C. K. (2018) Mineral paragenesis, fluid inclusions, H-O isotopes and ore-forming processes of the giant Dahutang W-Cu-Mo deposit, South China. *Ore Geol. Rev.* **99**, 116–150.
- Tagirov B. R., Zotov A. V. and Akinfiev N. N. (1997) Experimental study of dissociation of HCl from 350 to 500°C and from 500 to 2500 bars: thermodynamic properties of HCl⁰(aq). *Geochim. Cosmochim. Acta* **61**, 4267–4280.

- Testemale D., Brugger J., Liu W., Etschmann B. and Hazemann J.-L. (2009) In-situ X-ray absorption study of Iron(II) speciation in brines up to supercritical conditions. *Chem. Geol.* **264**, 295–310.
- Timofeev A., Migdisov A. A. and Williams-Jones A. E. (2017) An experimental study of the solubility and speciation of tantalum in fluoride-bearing aqueous solutions at elevated temperature. *Geochim. Cosmochim. Acta* **197**, 294–304.
- Vasyukova O. V. and Williams-Jones A. E. (2018) Direct measurement of metal concentrations in fluid inclusions, a tale of hydrothermal alteration and REE ore formation from Strange Lake, Canada. *Chem. Geol.* **483**, 385–396.
- Wang X.-S., Timofeev A., Williams-Jones A. E., Shang L.-B. and Bi X.-W. (2019) An experimental study of the solubility and speciation of tungsten in NaCl-bearing aqueous solutions at 250, 300, and 350 °C. *Geochim. Cosmochim. Acta* **265**, 313–329.
- Wang X., Qiu Y., Lu J., Chou I. M., Zhang W., Li G., Hu W., Li Z. and Zhong R. (2020) In situ Raman spectroscopic investigation of the hydrothermal speciation of tungsten: implications for the ore-forming process. *Chem. Geol.* **532** 119299.
- Webster J. D. (1990) Partitioning of F between H₂O and CO₂ fluids and topaz rhyolite melt. *Contrib. Mineral. Petrol.* **104**, 424–438.
- Wei W., Hu R., Bi X., Peng J., Su W., Song S. and Shi S. (2012) Infrared microthermometric and stable isotopic study of fluid inclusions in wolframite at the Xihuashan tungsten deposit, Jiangxi province, China. *Miner. Depos.* **47**, 589–605.
- Wesolowski D., Drummond S. E., Mesmer R. E. and Ohmoto H. (1984) Hydrolysis equilibria of tungsten(VI) in aqueous sodium-chloride solutions to 300-degrees-c. *Inorg. Chem.* **23**, 1120–1132.
- Williams-Jones A. and Migdisov A. (2014) Experimental constraints on the transport and deposition of metals in ore-forming hydrothermal systems. *Soc. Econ. Geol.* **18**, 77–96.
- Wood S. A. (1992) Experimental determination of the solubility of WO₃(s) and the thermodynamic properties of H₂WO₄(aq) in the range 300–600 C at 1 kbar: calculation of scheelite solubility. *Geochim. Cosmochim. Acta* **56**, 1827–1836.
- Wood S. A. and Samson I. M. (2000) The hydrothermal geochemistry of tungsten in granitoid environments: I. Relative solubilities of ferberite and scheelite as a function of T, P, pH, and m_{NaCl} . *Econ. Geol.* **95**, 143–182.
- Wood S. A. and Vlassopoulos D. (1989) Experimental determination of the hydrothermal solubility and speciation of tungsten at 500° C and 1 kbar1, 2. *Geochim. Cosmochim. Acta* **53**, 303–312.
- Wu M. Q., Samson I. M. and Zhang D. H. (2017) Textural and chemical constraints on the formation of disseminated granite-hosted W-Ta-Nb mineralization at the Dajishan Deposit, Nanling Range, Southeastern China. *Econ. Geol.* **112**, 855–887.
- Yang J.-H., Zhang Z., Peng J.-T., Liu L. and Leng C.-B. (2019) Metal source and wolframite precipitation process at the Xihuashan tungsten deposit, South China: insights from mineralogy, fluid inclusion and stable isotope. *Ore Geol. Rev.* **111** 102965.

Associate editor: Martin Reich